Title
Far-infrared VRT spectroscopy of the water dimer: Characterization of the 20 μm out-of-plane librational vibration

Journal
The Journal of Chemical Physics, 143(15)

ISSN
0021-9606

Authors
Cole, William TS
Fellers, Ray S
Viant, Mark R
et al.

Publication Date
2015-10-21

DOI
10.1063/1.4933116

Peer reviewed

AIP | The Journal of Chemical Physics

Far-infrared VRT spectroscopy of the water dimer: Characterization of the 20 μm out-of-plane librational vibration

William T. S. Cole, Ray S. Fellers, Mark R. Viant, Claude Leforestier, and Richard J. Saykally

Citation: The Journal of Chemical Physics **143**, 154306 (2015); doi: 10.1063/1.4933116
View online: http://dx.doi.org/10.1063/1.4933116
View Table of Contents: http://scitation.aip.org/content/aip/journal/jcp/143/15?ver=pdfcov
Published by the AIP Publishing

Far-infrared VRT spectroscopy of the water dimer: Characterization of the 20 μm out-of-plane librational vibration

William T. S. Cole,[1] Ray S. Fellers,[1,a)] Mark R. Viant,[1,b)] Claude Leforestier,[2] and Richard J. Saykally[1,c)]
[1]*Department of Chemistry, University of California, Berkeley, California 94705, USA*
[2]*Institut Charles Gerhardt UMR5253 CC15.01, CNRS and Universite Montpellier, 34095, Montpellier, Cedex 05, France*

(Received 17 August 2015; accepted 1 October 2015; published online 20 October 2015)

We report the first high-resolution spectra for the out-of-plane librational vibration in the water dimer. Three vibrational subbands comprising a total of 188 transitions have been measured by diode laser spectroscopy near 500 cm^{-1} and assigned to $(H_2O)_2$ libration-rotation-tunneling eigenstates. The band origin for the $K_a = 1$ subband is ~524 cm^{-1}. Librational excitation increases the interchange and bifurcation hydrogen bond rearrangement tunneling splittings by factors of 3-5 and 4-40, respectively. Analysis of the rotational constants obtained from a nonlinear least squares fit indicates that additional external perturbations to the energy levels are likely. © *2015 AIP Publishing LLC.* [http://dx.doi.org/10.1063/1.4933116]

INTRODUCTION

The study of water clusters with high-resolution spectroscopic methods has facilitated the determination of accurate potential energy surfaces for the water dimer, and more detailed models for bulk water.[1–9] A central objective of this research, and one which is actually nearing fruition, is the determination of a "predictive universal water model" capable of describing water in all its forms over wide ranges of conditions, based on the combination of high precision spectroscopic results and state-of-the-art *ab initio* calculations for small water clusters.[1,6,7,10–15] The most important step in this process is to obtain a "perfect" water dimer potential surface, since two-body forces account for ~90% of the total cohesive energy of solid and liquid water,[3,6,16] and the dominant many-body interactions (induction) are actually contained in the tensorial description of dimer polarization.[3,5] Three-body interactions will then be refined via similar procedures for the trimer, tetramer, etc.

Accurate description of water dimer spectra ultimately requires the solution of a 12-dimensional dynamics problem, comprising the six strongly coupled large-amplitude intermolecular motions and six intramolecular vibrations.[7,8,18,19] The experimentally determined "*trans*-linear" structure of the water dimer[17,20–23] is widely recognized as the archetype of hydrogen bonding.[24] Figure 1 depicts the 6 intermolecular vibrations along with the rotation-tunneling energy level diagram for a representative $(H_2O)_2$ $|J, K_a\rangle$ state. The complicated energy level diagram is a result of the 3 low-barrier tunneling pathways that connect the 8 degenerate minima on the 12-dimensinal water dimer potential energy surface.[25–27] At is the lowest barrier pathway (estimated at 157 cm^{-1} from the VRT(ASP-W) potential[2]) and is interpreted as the exchange of the two hydrogens in the acceptor molecule. Acceptor switching, At, tunneling splits the initial energy level of the dimer into two new levels, conventionally labeled A_1 and A_2. The second tunneling pathway, Interchange (It), comprises the exchange of the donor and acceptor molecules. Several pathways exist for this form of tunneling, but the lowest barrier path (207 cm^{-1}) is the "Geared" interchange. This tunneling motion further splits each A_1 or A_2 level into a triplet. The new energy levels are labeled by their representation in the G_{16} group. A final tunneling pathway, Bifurcation (Bi), is represented by the exchange of the hydrogen on the donor molecule. This pathway has the highest barrier (394 cm^{-1}) and results in an additional shift of the energy levels, but no new splittings. All of these tunneling motions are strongly coupled with the intermolecular vibrations and can produce non-trivial shifts/splittings (> a few cm^{-1}) accounting for the considerable complexity in the H_2O dimer spectra.[28–32] These tunneling motions, especially the (Bi) pathway, can be used to obtain dynamical information about the hydrogen bond.[33]

As we described in a recent review,[20] extensive high precision spectra have now been measured for all of these degrees of freedom-except two, which are actually the most important motions to fully characterize: the in-plane and out-of-plane librations. A short collection of the salient experimental results and recent theoretical predictions is given in Table I. Both librations are thought to be important in hydrogen bond dynamics, but the lack of laser sources at frequencies above 5 THz has limited progress. Both librations comprise motions that initiate the hydrogen bond breaking/formation processes in the condensed phases. Several theory groups have examined the importance of librations in the dynamics of the water hydrogen bond network, and studies of the H_2O trimer and larger

a)Present address: Yahoo, 3420 Central Expressway, Santa Clara, California 95051.
b)Present Address: Department of Biosciences, University of Birmingham, Edgbaston, Birmingham, UK.
c)Author to whom correspondence should be addressed. Electronic mail: saykally@berkeley.edu

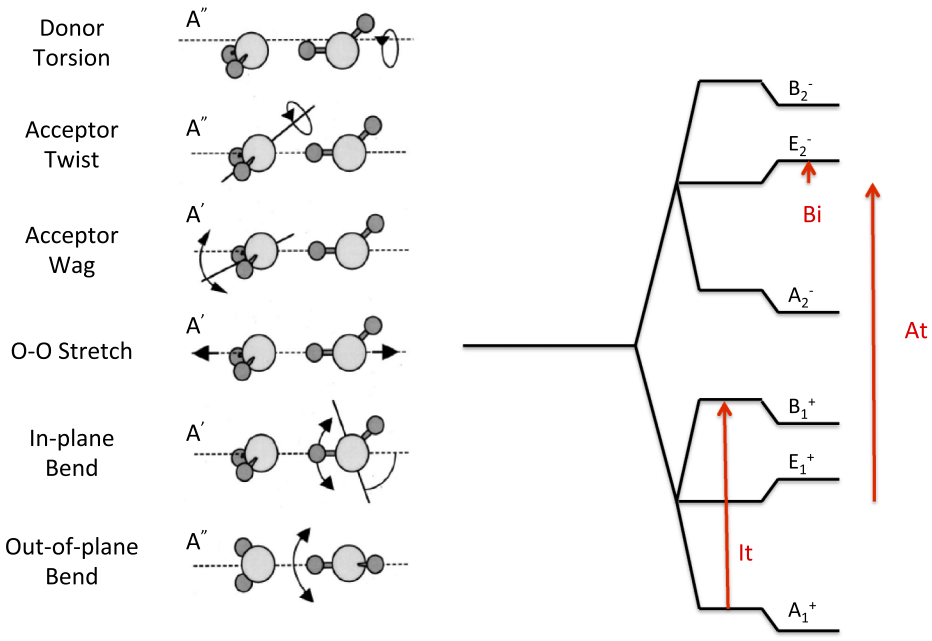

Rep.	E	(12) (34)	(ab)(13)(24) (ab)(14)(23)	(ab)(1324) (ab)(1423)	(12)(34)	E*	(12)* (34)*	(ab)(13)(24)* (ab)(14)(23)*	(ab)(1324)* (ab)(1423)*	(12)(34)*
A_1^+	1	1	1	1	1	1	1	1	1	1
A_2^+	1	-1	-1	1	1	1	-1	-1	1	1
B_1^+	1	1	-1	-1	1	1	1	-1	-1	1
B_2^+	1	-1	1	-1	1	1	-1	1	-1	1
E^+	2	0	0	0	-2	2	0	0	0	-2
A_1^-	1	1	1	1	1	-1	-1	-1	-1	-1
A_2^-	1	-1	-1	1	1	-1	1	1	-1	-1
B_1^-	1	1	-1	-1	1	-1	-1	1	1	-1
B_2^-	1	-1	1	-1	1	-1	1	-1	1	-1
E^-	2	0	0	0	-2	-2	0	0	0	2

FIG. 1. (Top left) The six intermolecular vibrations of $(H_2O)_2$. The labels by the molecules represent the symmetry of the vibration with respect to the molecular plane of symmetry. (Top right) A representative energy level for a state with $K_a = 0, J = 0$ and A′ vibrational symmetry. The symmetry of the energy levels is given by their representation in the group G_{16} as shown by Dyke.[17] The results of the three tunneling motions on the energy levels are also shown. Acceptor switching tunneling (At) splits a $|J, K_a\rangle$ level in to a set of two levels (denoted as 1's triplet and 2's triplet depending on the subscript of the symmetry label). Interchange tunneling (It) splits each of these two levels into a triplet. Bifurcation (Bi) tunneling further perturbs the levels but does not result in additional energy levels. (Bottom) The character table for the G_{16} symmetry group which characterizes the energy levels of the water dimer.

clusters have provided considerable insight.[34–38] In this paper, we present the first detailed experimental study of a libration in the $(H_2O)_2$ dimer, made in the librational band region of the liquid via far-infrared VRT spectroscopy.

EXPERIMENTAL

The Berkeley supersonic beam/diode laser spectrometer used in this study has been described in detail elsewhere[39–41] and only a short description will be provided here.

A helium-cooled diode laser spectrometer (Spectra Physics) using lead-salt diodes (Laser Photonics) was used to produce infrared radiation from 515 to 528 cm^{-1}. The beam was multipassed 18-22 times through a pulsed planar supersonic expansion of a mixture of H_2O and He using a Herriot cell and detected using a helium cooled (Si:B) photoconductive detector (IR Labs). The supersonic expansion is produced by bubbling pure He gas, with a backing pressure of 1-2 atm, through liquid H_2O, and then through a 101.6 mm long slit at a repetition rate of 35 Hz into a

TABLE I. Previously measured and calculated VRT levels and tunneling splittings of $(H_2O)_2$.[a]

		Experiment	HBB2	CCpol-8s/f	MB-pol		Experiment	HBB2	CCpol-8s/f	MB-pol
OO	(2)	153.62(1.88)	148.57(1.14)	149.63(1.23)	154.31(2.41)	(1)		152.50(1.12)	152.07(1.48)	156.60(2.71)
	(1)		145.00(3.48)	143.20(3.27)	149.44(1.97)	(2)		150.52(1.04)	153.54(2.54)	152.69(4.13)
AT	(1)		128.91(0.74)	132.10(1.48)	129.44(0.24)	(1)		142.25(4.33)	142.42(4.04)	143.68(4.87)
	(2)	120.19(9.39)	121.01(8.41)	117.50(8.67)	119.07(10.15)	(2)		136.24(5.31)	136.52(4.66)	137.04(5.95)
AW	(2)	108.89(0.02)	105.78(0.03)	107.82(0.10)	108.87(0.13)	(2)	123.56(3.41)	122.25(2.48)	123.12(3.16)	123.65(3.83)
	(1)	107.93(2.95)	105.35(1.99)	109.23(3.29)	108.38(3.24)	(1)	109.98(5.24)	108.95(4.55)	108.28(4.76)	109.65(5.89)
DT	(1)		116.54(4.84)	113.35(5.91)	113.83(5.61)	(2)		94.25(2.66)	92.18(3.34)	91.22(3.47)
	(2)	64.52(2.54)	67.18(2.03)	61.33(2.48)	61.31(2.54)	(1)	87.75(1.11)	89.55(0.54)	86.37(1.32)	85.63(1.00)
GS	(2)	11.18(0.65)	10.16(0.60)	12.75(0.61)	12.05(0.69)	(1)	14.39(0.70)	14.00(0.64)	15.45(0.67)	15.04(0.77)
	(1)	0.00(0.75)	0.00(0.68)	0.00(0.72)	0.00(0.81)	(2)	11.66(0.54)	11.50(0.49)	12.36(0.51)	12.18(0.48)
			$K_a = 0$					$K_a = 1$		

[a]The observed and predicted values of the VRT levels of the intermolecular vibrations of $(H_2O)_2$. Ground State (GS), Donor Torsion (DT), Acceptor Wag (AW), Acceptor Twist (AT), intermolecular stretch (OO) intermolecular energy levels are shown. The labels (1) and (2) correspond to the energies (cm^{-1}) of the origin of the intermolecular vibration's 1's triplet or 2's triplet, respectively (see Figure 1). The values in parentheses are the interchange tunneling splittings of the corresponding triplet. Reproduced with permission from Babin *et al.*, J. Chem. Theory Comput. **9**, 5395–5403 (2013). Copyright 2013 American Chemical Society.

vacuum chamber maintained at ~200 mTorr by a Roots blower (Edwards 4200) backed by two rotary pumps (E2M 275). The cooling in the supersonic beam was sufficient for the cluster species to reach a rotational temperature of 4 K. Simultaneously, the fringe spacing of a vacuum-spaced etalon and an OCS (carbonyl sulfide) reference gas spectrum is detected with a liquid He cooled (Cu:Ge) detector (Santa Barbara Research Center) and recorded to enable precise frequency calibration. The observed linewidths of ~30 MHz full-width half maximum (FWHM) are slightly larger than the Doppler limited linewidths extrapolated form earlier experiments. Typical frequency accuracy is 10-20 MHz, which was limited by linewidths of the cluster absorptions and laser drift.

Spectra are detected in direct absorption using a time-gated phase sensitive signal processing approach. The sensitivity of the experiment has been previously discussed by Keutsch *et al.*:[42] briefly, the signal-to-noise ratio of the Q-branches was about 200:1 compared to 8000:1 for the most intense vibrations observed in THz experiments performed in the same group. The sensitivity of the diode laser experiment (10-100 ppm) is about 2 orders of magnitude lower than that of the THz experiments, indicating that the observed transitions are intense.

Accessing the 500 cm^{-1} region of the electromagnetic spectrum has been notoriously difficult. The first observation of a libration in the region was reported in 1987 by von Puttkamer and Quack.[43] The spectra reported here required the use of 10 separate laser diodes, each scanned across several modes to cover the specified spectral range. However, large laser gaps are nevertheless present in the spectra, which cause considerable difficulty in the assignment. It is relevant to note that Keutsch *et al.* have previously assigned a portion of the measured raw experimental spectrum to librations of the H_2O trimer.[42] Recent matrix isolation results from the Lund group prompted a reinvestigation of the remaining unassigned lines in that region.[44–47] Figure 2 shows the region of the experimental study with respect to the librational band of liquid water, along with the assigned dimer transitions and the remaining unassigned lines. Figure 3 presents actual spectra observed in a small region, wherein the dimer lines assigned in this regions are much weaker than the dominant trimer lines assigned in Ref. 42.

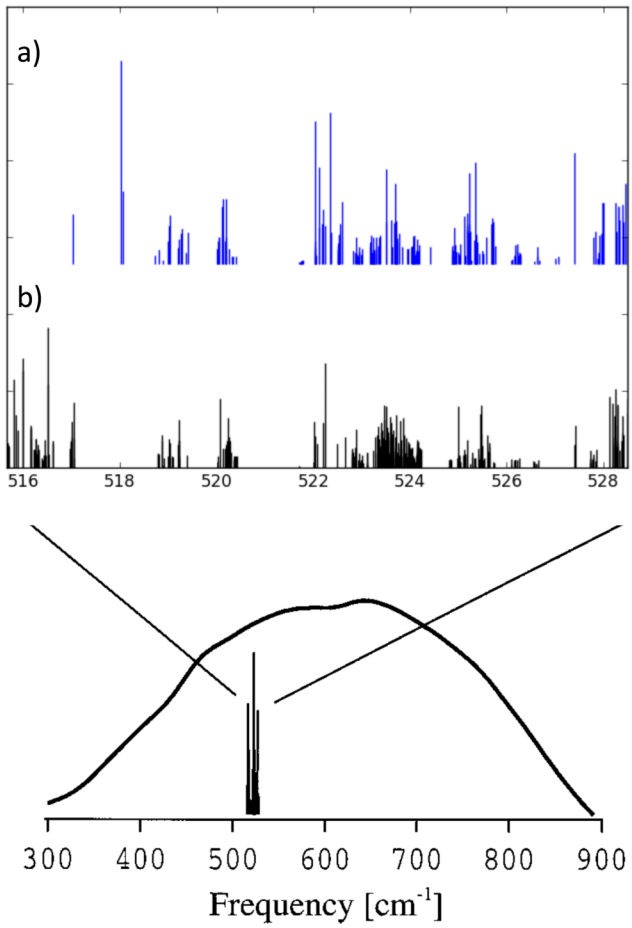

FIG. 2. The librational band of liquid water is shown along with the measured dimer transitions. (a) Shows the assigned lines presented in this study. (b) The remaining unassigned transitions in the region. The spectrum has significant laser gaps, which cause difficulty in the assignment. Spectra were collected from a He:H_2O expansion in a pulsed, supersonic jet. Linewidths are ca. 30 MHz, and frequency accuracy is 10-20 MHz.

RESULTS

Assignment

189 transitions comprising the experimentally observed spectrum have been assigned to an excited vibrational state with A″ symmetry; the transitions terminate in three distinct subbands designated by their K_a value; the upper state subbands observed here involve K_a = 0, 1, and 2. 55 transitions are assigned as a-type ($\Delta K_a = 0$), 110 transitions are assigned to b-type ($\Delta K_a = +1$), 23 are assigned to "c"-type transitions ($\Delta K_a = -1$), and one transition is assigned to a H_2O monomer. As a note, the labeling of transitions as "c"-type is merely one of convenience to separate those transitions from the rest of the b-type transitions. The selection rules that dictate the assignment are conventional. One of the following must hold: $\Delta J \neq 0$, $\Delta K_a \neq 0$, $\Delta K_c \neq 0$, and additionally, transitions from a state with a given symmetry label must terminate in a level with the same symmetry but with a change in parity (i.e., $A_2^+ \rightarrow A_2^-$). These selection rules dictate the possible observable transitions.[17]

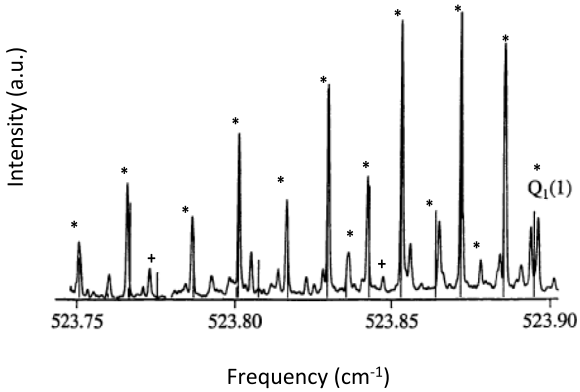

FIG. 3. A small portion of the spectral region covered in this study. Asterisks indicate transitions previously assigned to the much stronger out-of-plane libration of the H_2O trimer.[42] The + labels represent the two dimer transitions observed in the region.

Transitions were assigned through the use of pattern recognition algorithms and ground state combination differences. Intensity patterns were also compared to predictions using the spin statistical weights of each symmetry species, but as the power output of the diode laser was quite variable, they could not be used in every case. The presence of Q-branches was used to confirm the results, along with the agreements of the rotational constants from the fit. Some missing transitions hindered assignment of more transitions due to the significant laser gaps in the spectrum.

A brief discussion of notation

For the sections that follow, a description of the notation that will be used is helpful. For Table I, the transitions are grouped into "sets" which represent transitions to the same "frequency location" in the upper state, referring to the energy level diagram for the H_2O dimer (Fig. 1). For example, the A_2^-/B_2^+ "set" refers to the transitions which originate in an eigenstate with symmetry A_2^- or B_2^+ and terminate in one with symmetry A_2^+ or B_2^-, respectively. The first symmetry in the label of each "set" corresponds to the symmetry of the lowest possible eigenstate for a given set, noting that this depends on the type of transition. For example, if the transition type is $K_a = 1 \leftarrow 1$ and one considers the set A_2^-/B_2^+, this means that the lowest energy ground state is labeled A_2^-, and that the labels alternate with increments of 1 in J. The reason we group transition in this manner is because the sets originate and terminate in the same relative frequency locations in a given triplet. Returning to our example of the $K_a = 1 \leftarrow 1$ transition in the set A_2^-/B_2^+, the transitions originate in the lowest level of the ground state triplet and terminate in the top level of the upper state triplet. This system greatly simplifies not only the assignment procedure but also the fitting process.

Analysis

The measured K_a subbands were fit to the following near-prolate top energy expressions as described previously:[30,48]

$K_a = 0$,

$$E\left(A^{\pm} or B^{\pm}\right) = v^{(0)} \pm \left(\frac{It^{(0)}}{2}\right) - v_{Bi}^{(0)} + B^{(0)}J(J+1) - D^{(0)}(J(J+1))^2, \quad (1)$$

$$E\left(E^{\pm}\right) = v^{(0)} + v_{Bi}^{(0)} + B^{(0)}J(J+1) - D^{(0)}(J(J+1))^2, \quad (2)$$

$K_a = 1$,

$$E\left(A^{\pm} or B^{\pm}\right) = v^{(1)} \pm \left(\frac{It^{(1)}}{2}\right) + v_{Bi}^{(1)} + B^{(1)}(J(J+1)-1) - D^{(1)}(J(J+1)-1)^2 \pm \left[\left(\frac{B-C}{4}\right)^{(1)} - d^{(1)}J(J+1)\right]J(J+1), \quad (3)$$

$$E\left(E^{\pm}\right) = v^{(1)} - v_{Bi}^{(1)} + B^{(1)}(J(J+1)-1) - D^{(1)}(J(J+1)-1)^2 \pm \left[\left(\frac{B-C}{4}\right)^{(1)} - d^{(1)}J(J+1)\right]J(J+1). \quad (4)$$

$K_a = 2$,

$$E\left(A^{\pm} or B^{\pm}\right) = v^{(2)} \pm \left(\frac{It^{(2)}}{2}\right) - v_{Bi}^{(2)} + B^{(2)}(J(J+1)-4) - D^{(2)}(J(J+1)-4)^2 \pm \left[\left(\frac{B-C}{4}\right)^{(2)}\right]J(J+1)(J-1)(J+2), \quad (5)$$

$$E\left(E^{\pm}\right) = v^{(2)} + v_{Bi}^{(2)} + B^{(2)}(J(J+1)-4) - D^{(2)}(J(J+1)-4)^2 \pm \left[\left(\frac{B-C}{4}\right)^{(2)}\right]J(J+1)(J-1)(J+2). \quad (6)$$

In these expressions, $v^{(i)}$, B, D, and (B-C)/4 have their usual meanings. The constant $d^{(1)}$ is an additional centrifugal distortion constant previously shown to improve fitting of the $K_a = 1$ levels and is a manifestation of the non-rigidity of the complex. The tunneling splittings are defined as shown in Figure 1. It is the separation of the $A^{\pm}$ and $B^{\pm}$ levels in a particular triplet, and bifurcation (v_{Bi}) is a shift of each energy level in the triplet. Acceptor switching splitting is not determined explicitly from the fit but can easily be obtained when the origins of the $E^{\pm}$ for both the 1's and 2's triplets are known by

$$Acceptor\ Switching(AS)^{(i)} = \left|v_{1's}^{(i)}(E^{\pm}) - v_{2's}^{(i)}(E^{\pm})\right|. \quad (7)$$

The assigned transitions are shown in Table II along with the differences between the observed transitions frequencies and those calculated from the constants obtained from the fit. Table III shows the constants obtained from a nonlinear least squares fit of all the transitions to the expressions given in Equations (1)-(6) along with the 1σ deviations. The root mean squared deviation of the fit is found to be ~12 MHz, which is well within the frequency accuracy of the experiment. The fit was performed holding the known ground state parameters fixed to calculate the lower state energy. One fit was performed without the parameters fixed and showed good agreement with the known ground state constant values, indicating that the transitions originated in the vibrational ground state. Results of the fit including correlation matrices are provided in the supplementary material.[49]

The c-type $K_a = 0 \leftarrow 1$ subband

23 lines were assigned to transitions originating in $K_a = 1$ of the ground state and terminating in the $K_a = 0$ excited state. These transitions represent only the 1's triplet of the $K_a = 0$ stack and thus render it impossible to determine the acceptor switching splitting of the upper state. Significant laser gaps

TABLE II. Assigned experimental transitions. All values are given in MHz. The symmetry labels represent the lower state symmetry. The type of transition is shown along with the transition frequency and the difference between observed and calculated transition frequencies. The explicit upper (J′) and lower (J″) J quantum numbers are shown.

K = 1 ← 0

			A_1^+/B_1^-		E_1^+/E_1^-		B_1^+/A_1^-	
Transition type	J′	J″	Frequency	Obs − calc	Frequency	Obs − calc	Frequency	Obs − calc
R(6)	7	6			15 754 572.8	0.3		
R(3)	4	3			15 715 103.6	0.0		
R(2)	3	2			15 702 326.3	2.4		
R(0)	1	0			15 677 366.1	0.5		
P(2)	1	2			15 640 633.4	−1.8		
P(6)	5	6			15 592 917.1	−1.5		
P(9)	8	9			15 559 477.4	0.0		
			A_2^-/B_2^+		E_2^-/E_2^+		B_2^-/A_2^+	
Transition type	J′	J″	Frequency	Obs − calc	Frequency	Obs − calc	Frequency	Obs − calc
R(0)	1	0	15 750 564.6	−2.9	15 748 926.0	−5.2	15 679 580.0	−10.0
R(2)	3	2	15 775 602.9	−1.4	15 773 810.0	−2.5	15 704 545.1	−8.6
R(3)	4	3	15 788 407.1	−2.2	15 786 438.9	−1.6		
R(4)	5	4	15 801 295.9	−3.3	15 799 208.3	−1.4		
R(5)	6	5					15 742 698.1	−8.2
R(6)	7	6	15 828 089.2	−14.8	15 825 747.1	−8.5	15 756 185.8	−10.6
R(7)	8	7	15 841 336.0	−19.2	15 839 040.3	−11.4		
Q(1)	1	1	15 737 611.4	3.3	15 735 784.7	2.9	15 664 927.8	−7.7
Q(2)	2	2	15 737 247.6	9.0	15 735 561.9	7.1	15 664 878.2	−6.9
Q(3)	3	3	15 736 875.8	15.8	15 735 486.8	10.8	15 664 847.3	−5.9
Q(4)	4	4	15 736 354.4	25.0	15 735 367.3	15.8	15 664 700.7	−4.7
Q(5)	5	5	15 735 927.4	30.8			15 664 514.8	−3.9
P(2)	1	2	15 713 557.5	−2.9	15 712 190.4	−7.8	15 642 750.7	−1.0
P(3)	2	3	15 701 333.9	−1.9	15 700 004.3	−7.3		
P(4)	3	4	15 689 410.9	−2.8				
P(5)	4	5	15 677 487.0	−2.9	15 675 832.8	−5.3		
P(6)	5	6	15 665 946.3	−6.2	15 664 355.5	−9.0	15 594 831.1	−8.2
P(7)	6	7	15 654 757.3	−12.5	15 652 694.5	−10.0		
P(8)	7	8			15 641 331.7	−13.1	15 571 664.1	−1.1
P(9)	8	9					15 560 163.6	−14.5

K = 1 ← 1

			A_2^-/B_2^+		E_2^-/E_2^+		B_2^-/A_2^+	
Transition type	J′	J″	Frequency	Obs − calc	Frequency	Obs − calc	Frequency	Obs − calc
R(9)	10	9					15 753 818.4	25.5
R(8)	9	8	15 837 385.9	−11.6	15 840 653.3	−11.5	15 740 516.3	9.1
R(7)	8	7	15 824 326.9	8.5	15 826 791.1	12.4		
R(6)	7	6	15 811 272.5	−6.3			15 714 101.7	18.9
R(5)	6	5					15 701 175.4	21.5
R(4)	5	4					15 688 318.2	21.3
R(3)	4	3	15 772 309.4	2.9	15 774 399.1	6.9		
R(2)	3	2	15 759 746.4	−2.4				
R(1)	2	1	15 747 330.1	−3.9	15 749 418.1	0.4	15 650 663.8	19.4
P(2)	1	2	15 698 247.7	−9.3	15 700 298.7	−4.3	15 601 381.0	1.9
P(3)	2	3	15 686 055.4	−4.9	15 688 103.4	−0.2		
P(4)	3	4	15 674 001.0	−8.4				
P(5)	4	5					15 565 354.7	2.1
P(6)	5	6	15 650 333.3	−9.8	15 652 772.0	−8.4		
P(7)	6	7			15 641 190.5	6.3		
P(8)	7	8					15 530 889.3	1.7

TABLE II. (*Continued.*)

K = 1 ← 1								
			B_2^+/A_2^-		E_2^+/E_2^-		A_2^+/B_2^-	
Transition type	J′	J″	Frequency	Obs − calc	Frequency	Obs − calc	Frequency	Obs − calc
R(9)	10	9	15 842 745.8	0.0	15 842 869.4	0.0	15 750 087.9	4.5
R(8)	9	8	15 829 080.9	14.6	15 828 609.8	3.3		
R(7)	8	7					15 721 674.1	−13.5
R(6)	7	6					15 707 891.5	0.0
R(5)	6	5			15 789 415.5	−0.1	15 694 142.9	−17.9
R(4)	5	4	15 777 453.7	1.2	15 776 722.3	2.6		
R(2)	3	2	15 752 316.7	0.9				
R(1)	2	1	15 739 942.6	4.4	15 739 155.8	−1.2	15 641 477.8	−11.9
P(2)	1	2	15 690 947.8	−1.5	15 689 757.2	−0.2	15 590 663.7	−0.9
P(3)	2	3	15 678 765.8	−0.7	15 677 531.4	1.4		
P(4)	3	4	15 666 802.3	−3.0			15 565 602.3	0.2
P(5)	4	5	15 655 013.8	−1.3			15 553 293.1	16.3
P(6)	5	6			15 641 637.6	−2.6		
P(7)	6	7					15 529 855.5	23.2
P(10)	9	10	15 599 103.7	−14.7	15 595 341.1	−3.3		
K = 0 ← 1								
			A_1^+/B_1^-		E_1^+/E_1^-		B_1^+/A_1^-	
Transition type	J′	J″	Frequency	Obs − calc	Frequency	Obs − calc	Frequency	Obs − calc
R(10)	11	10					15 762 015.3	−3.2
R(8)	9	8			15 777 584.0	3.6		
R(6)	7	6			15 751 154.7	5.4	15 709 915.7	−7.8
R(5)	6	5	15 838 541.2	−24.6				
R(3)	4	3			15 711 967.3	6.0		
R(2)	3	2			15 699 305.3	4.3	15 659 376.1	−4.4
R(1)	2	1	15 787 937.9	−11.4	15 686 891.2	1.0		
Q(2)	2	2	15 760 894.9	12.3				
Q(4)	4	4	15 760 674.4	17.1				
Q(6)	6	6	15 760 462.2	16.4				
Q(8)	8	8	15 760 024.2	3.5				
P(1)	0	1	15 750 273.0	−7.0	15 650 150.4	−5.7		
P(2)	1	2					15 596 676.9	5.4
P(5)	4	5	15 700 772.0	−0.6				
P(6)	5	6			15 590 454.5	−4.4		
P(7)	6	7	15 676 366.2	−5.7				
P(8)	7	8			15 567 303.4	−3.6		
P(9)	8	9			15 555 922.3	−6.6		
P(10)	9	10					15 500 205.9	10.1
K = 2 ← 1								
			A_2^-/B_2^+		E_2^-/E_2^+		B_2^-/A_2^+	
Transition type	J′	J″	Frequency	Obs − calc	Frequency	Obs − calc	Frequency	Obs − calc
R(9)	10	9					15 760 674.4	−0.4
R(8)	9	8					15 746 844.1	−17.2
R(6)	7	6	15 838 543.5	−4.1	15 775 891.9	−3.5		
R(5)	6	5	15 825 488.9	−29.8			15 707 184.1	3.0
R(4)	5	4			15 749 526.1	−1.0	15 694 202.9	−2.6
R(1)	2	1	15 774 243.4	−12.2	15 711 420.7	−11.7	15 656 398.1	−0.9
Q(2)	2	2	15 746 176.3	21.0	15 684 814.1	7.1		
Q(3)	3	3	15 746 115.5	22.1	15 684 702.1	4.7		
Q(4)	4	4	15 746 021.7	16.3	15 684 661.5	−20.5		
Q(6)	6	6	15 745 594.0	20.0				
Q(7)	7	7	15 745 144.8	4.7				
P(3)	2	3	15 712 865.1	−12.2	15 650 085.5	−12.0	15 594 734.6	2.1
P(4)	3	4	15 700 643.7	−20.3				
P(6)	5	6	15 676 745.2	−22.4			15 558 912.2	−5.4

TABLE II. (*Continued.*)

K = 2 ← 1								
			A_2^-/B_2^+		E_2^-/E_2^+		B_2^-/A_2^+	
Transition type	J′	J″	Frequency	Obs − calc	Frequency	Obs − calc	Frequency	Obs − calc
P(7)	6	7	15 665 086.1	−20.5				
P(8)	7	8			15 590 090.8	−3.4		
P(9)	8	9	15 642 440.9	−12.1				
P(10)	9	10			15 567 527.9	−8.9		
			B_2^+/A_2^-		E_2^+/E_2^-		A_2^+/B_2^-	
Transition type	J′	J″	Frequency	Obs − calc	Frequency	Obs − calc	Frequency	Obs − calc
R(8)	9	8					15 749 638.8	0.0
R(6)	7	6	15 836 359.2	−32.2	15 776 419.7	−13.4		
R(5)	6	5	15 823 020.9	−12.2			15 710 644.5	3.4
R(4)	5	4			15 750 132.0	−11.7	15 697 736.6	0.0
R(1)	2	1	15 772 550.6	−17.7	15 712 009.0	−3.7	15 660 008.2	1.1
Q(2)	2	2	15 745 019.0	12.6	15 686 817.7	3.5		
Q(3)	3	3	15 744 987.5	16.5	15 686 790.7	−0.8		
Q(4)	4	4	15 744 864.0	27.1	15 686 419.9	8.9		
Q(5)	5	5	15 744 680.3	29.5	15 685 858.9	0.4		
Q(6)	6	6			15 685 227.0	29.8		
Q(8)	8	8	15 743 640.8	18.3				
P(3)	2	3	15 711 240.2	−21.4	15 650 478.8	−5.1	15 598 580.3	−1.1
P(5)	4	5	15 686 988.7	−14.7				
P(6)	5	6	15 674 973.0	−5.7				
P(7)	6	7					15 551 154.9	−3.4
P(8)	7	8			15 592 349.9	−12.3		
P(10)	9	10			15 570 108.0	4.3		

hindered assignment of the B_1^+/A_1^- set (for example, the region where the Q-branch is expected to reside falls in a large gap); however, sufficient transitions were assigned to unambiguously ascribe the spectra to a state with A″ vibrational symmetry. The results of the fit are shown in Table II. Transitions from the ground state $K_a = 1$, 2's triplet to the 2's triplet of the upper state $K_a = 0$ stack were also searched for but were not found. A possible explanation for this is that the transitions lie outside the experimental range due to the presumed large acceptor switching tunneling of the upper state; this will be elaborated in a later section.

The b-type $K_a = 1 \leftarrow 0$ subband

A total of 53 lines were assigned to transitions originating in the $K_a = 0$ ground state and ending in $K_a = 1$ excited state. Complete assignment of the excited state $K_a = 1$, 2's triplet was accomplished and, in combination with the transitions assigned in the subsection titled The a-type $K_a = 1 \leftarrow 1$ subband, allowed a detailed characterization of this manifold. The resulting energy level diagram shown in Figure 4 for all observed transitions confirms the vibrational symmetry of the upper state as A″. Additionally, the $E^{\pm}$ levels of the 1's triplet were found. While this may appear arbitrary without accompanying $A_1^{\pm}$ and $B_1^{\pm}$ transitions, the assignment was confirmed by ground state combination differences. Also the fingerprint of the $A_1^{\pm}$ and $B_1^{\pm}$ transitions was found; however, significant laser gaps precluded the observation of a suitable number of transitions for an unambiguous assignment. Nevertheless, the assignment of the $E^{\pm}$ transitions provides valuable insight into the acceptor switching in the upper state $K_a = 1$ stack. A full discussion of the observed tunneling splittings will be presented below.

The a-type $K_a = 1 \leftarrow 1$ subband

A total of 55 lines were assigned to a-type transitions originating and terminating in $K_a = 1$ stacks. All assigned transitions correspond to the 2's triplet of the upper state, and in conjunction with the assignments of the subsection titled The b-type $K_a = 1 \leftarrow 0$ subband, completely characterize the 2's triplet of the upper state $K_a = 1$ subband. This characterization reinforces the assignment of the state as having A″ vibrational symmetry. One striking feature of the fit results is the large magnitude of the D and d rotational constants for the B_2^-/A_2^+, which indicates a deviation from the semirigid near-prolate top energy level approximation. Also, the A_2^-/B_2^+ set's asymmetry constant displays an abnormal 1σ value, which may be an indication of some perturbation of that energy level set. Given that the quality of the fit is still very good, a possible explanation for this may engender the close proximity of the 2's of the $K_a = 1$ upper state stack to the 2's of the upper stack $K_a = 2$ stack, which is elaborated in the subsection titled The b-type $K_a = 2 \leftarrow 1$ subband.

TABLE III. Results from least squares fit of assigned transitions. All values are given in MHz. The symmetry labels indicate the lower state symmetry.

K = 0

A_1^+/B_1^-			E_1^+/E_1^-			B_1^+/A_1^-		
Constant	Value	1σ error	Constant	Value	1σ error	Constant	Value	1σ error
B	6 209.573	0.563	B	6236.608	0.494	B	6169.874	0.405
D	0.911	0.008	D	0.211	0.006	D	0.144	0.003
Origin	15 939 224.0	5.2						
Interchange tunneling	119 086.9	12.7						
Bifurcation tunneling	−15 553.0	5.2				Number of transitions in fit		23
RMS of fit	9.2							

K = 1

E_1^+/E_1^-		
Constant	Value	1σ error
B	6 200.3538	0.28
D	−0.3622	0.0042
(B-C)/4	−9.2627	0.18
d	−0.1821	0.0032
Origin	15 510 412.4	1.3
Interchange tunneling	n/a	
Bifurcation tunneling	n/a	

A_2^-/B_2^+			E_2^-/E_2^+			B_2^-/A_2^+		
Constant	Value	1σ error	Constant	Value	1σ error	Constant	Value	1σ error
B	6 217.946	0.235	B	6221.564	0.228	B	6270.691	1.805
D	0.064	0.031	D	0.057	0.029	D	2.141	0.019
(B-C)/4	4.557	1.414	(B-C)/4	5.255	0.144	(B-C)/4	11.126	0.119
d	0.161	0.023	d	0.028	0.022	d	1.027	0.016
Origin	15 890 455.7	1.9						
Interchange tunneling	61 510.0	4.4						
Bifurcation tunneling	−19 983.6	1.9	Acceptor tunneling		380 043.3			

B_2^+/A_2^-			E_2^+/E_2^-			A_2^+/B_2^-		
Constant	Value	1σ error	Constant	Value	1σ error	Constant	Value	1σ error
B	6 196.223	0.776	B	6178.346	0.500	B	6133.107	0.987
D	−0.019	0.007	D	−0.163	0.005	D	−2.150	0.016
(B-C)/4	−40.026	0.427	(B-C)/4	−17.946	0.316	(B-C)/4	−88.450	0.774
d	−0.333	0.004	d	−0.078	0.003	d	−1.673	0.014
Origin	15 876 498.2	5.2						
Interchange tunneling	83 884.9	12.6						
Bifurcation tunneling	−23 807.2	5.2				Number of transitions in fit		108
RMS of fit	10.1							

K = 2

A_2^-/B_2^+			E_2^-/E_2^+			B_2^-/A_2^+		
Constant	Value	1σ error	Constant	Value	1σ error	Constant	Value	1σ error
B	6 105.144	1.086	B	6197.430	1.292	B	6195.007	1.020
D	−1.566	0.018	D	5.763	0.109	D	−0.090	0.010
(B-C)/4	−0.442	0.004	(B-C)/4	−5.660	0.111	(B-C)/4	−0.111	0.002
Origin	15 892 966.0	9.0						
Interchange tunneling	100 704.6	21.2						
Bifurcation tunneling	−2 895.4	9.0						

TABLE III. (*Continued.*)

K = 2								
B_2^+/A_2^-			E_2^+/E_2^-			A_2^+/B_2^-		
Constant	Value	1σ error	Constant	Value	1σ error	Constant	Value	1σ error
B	6 268.086	1.139	B	6128.279	0.708	B	6166.044	1.369
D	1.732	0.022	D	−0.322	0.017	D	−0.554	0.022
(B-C)/4	−0.329	0.007	(B-C)/4	0.499	0.013	(B-C)/4	−0.410	0.008
Origin	15 894 035.5	7.3						
Interchange tunneling	94 285.6	19.3						
Bifurcation tunneling	−2 529.2	7.3				Number of transitions in fit		57
RMS of fit	14.3							

The b-type $K_a = 2 \leftarrow 1$ subband

A total of 57 lines were assigned to transitions from $K_a = 1$ in the ground state to the excited state $K_a = 2$ levels of an A″ vibration. The transitions completely characterize the 2's triplet and also reveal an interesting energy level structure between the 2's of the $K_a = 1$ stack and the 2's of the $K_a = 2$ stack. The difference between the origins of the $K_a = 1$ and $K_a = 2$ stacks is less than 1 cm^{-1} for all four stacks (considering the K doublets as separate stacks) and less than 5000 MHz for three of the triplets. This near-degeneracy, in addition with previously mentioned irregularities in the rotational constants, warranted an investigation into the possibility of Coriolis coupling between the levels, as has previously been shown to be significant for certain energy levels.[50]

Coriolis coupling is a result of $K_{a/c}$ not being a strictly "good" quantum number for the water dimer and allows levels of the same symmetry, parity, and J value to mix when brought into close proximity. The interaction generally follows a simple 2-level Coriolis resonance model.[30,50] After extensive investigation, the energy levels were actually found to **not** be strongly Coriolis coupled. An attempt to fit to the standard Coriolis

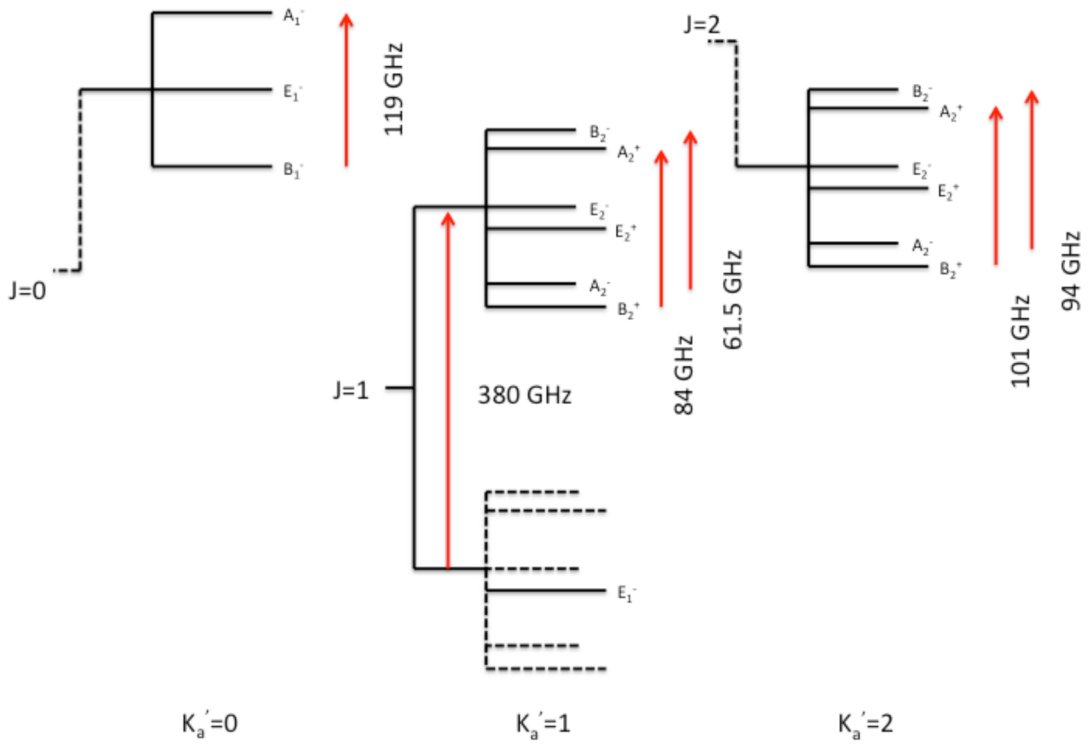

FIG. 4. Energy level diagram for the assigned transitions. Determined interchange and acceptor switching tunneling values are shown. Dashed lines represent the group theoretical structure for energy levels not determined from the current study. The energy level structure represents a A″ upper state vibration, consistent with the out-of-plane intermolecular libration. The origins of the 2's of the $K_a = 1$ and $K_a = 2$ stack lie in extreme proximity, which suggests that the levels may perturb each other. The bifurcation tunneling is not shown on this figure; however, the sign changes from $K_a = 0$ to $K_a = 1$ as expected and then changes sign from $K_a = 1$ to $K_a = 2$. Drawing not to scale.

model,

$$E = \frac{E^{(i)} + E^{(j)}}{2} \pm \left[\frac{\left(E^{(j)} - E^{(i)}\right)^2}{4} + \frac{\zeta^2 J(J+1)}{2} \right]^{1/2}, \quad (8)$$

wherein the i-th and j-th energies are obtained from the unperturbed energy expressions from Equations (1)-(6), produced values for the coupling parameter, $\zeta << 1$ MHz, whereas previously determined values for the parameter have been >1400 MHz. From this result, we conclude that Coriolis coupling is not a significant effect in the energy levels concerned.

This unusual result can be rationalized by considering the large magnitude of the interchange and bifurcation tunneling splittings, which keep the levels capable of mixing sufficiently isolated from each other. Figure 5 portrays the separation of the six possible sets that are capable of Coriolis interaction for a given J.

The figure illustrates that while the origins of the two stacks are very close, the large tunneling splitting in this state (particularly for the $K_a = 1$ stack) render the levels capable of Coriolis interaction so widely separated that the mixing is insignificant. Even for the sets that lie closest in proximity (the B_2^-/A_2^+ set and the A_2^+/B_2^- set), no appreciable Coriolis perturbation was found.

Vibrational assignment

Assignment of the energy level stacks to an A″ vibrational symmetry was unambigiously accomplished by observing the

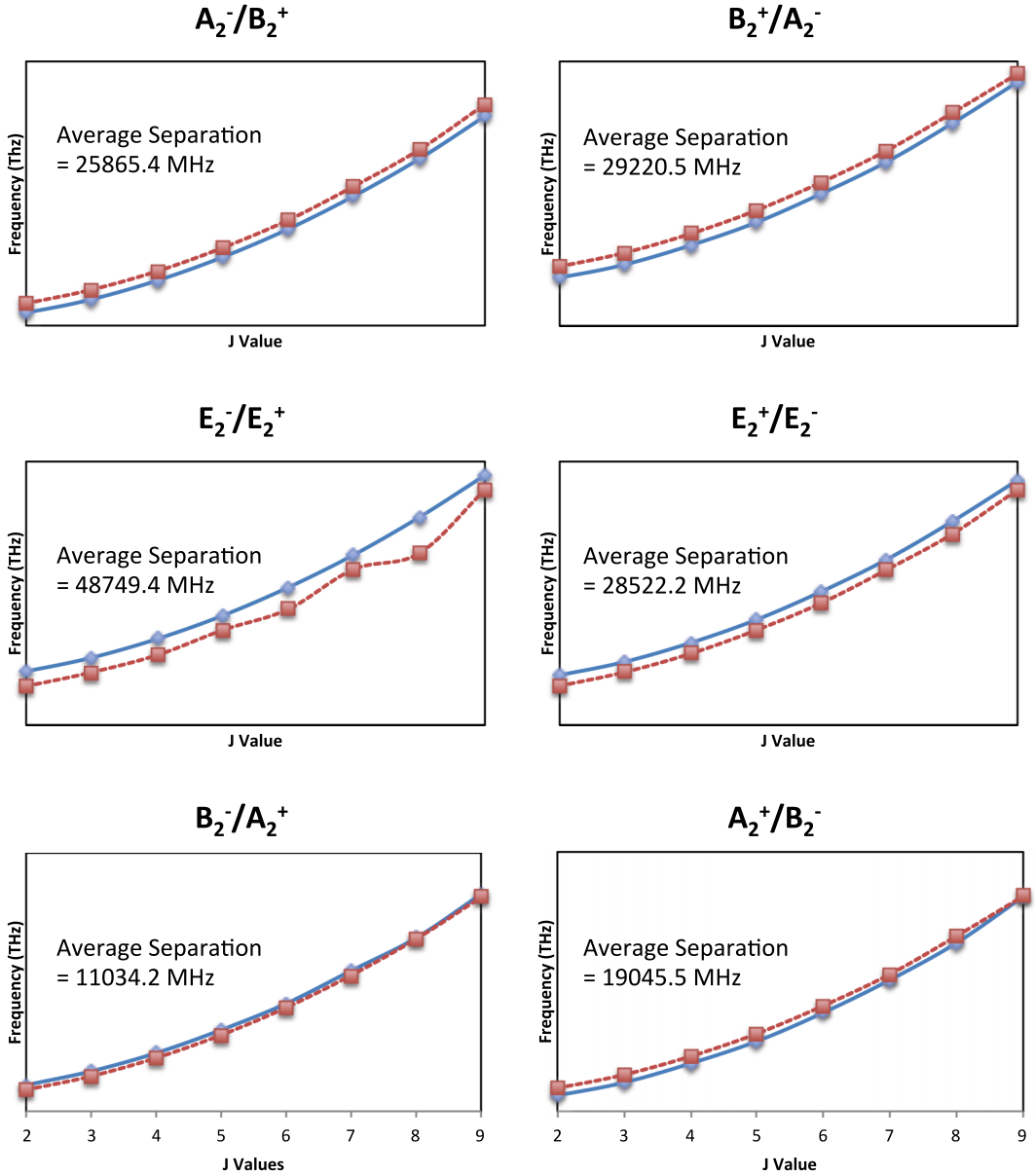

FIG. 5. Calculated energy levels for the 2's triplets of the $K_a = 1$ and $K_a = 2$ upper state stacks. Each plot is arranged so that the levels capable of participating in Coriolis coupling are plotted together. The calculated energies for the $K_a = 1$ stack are shown in blue/solid line, and the $K_a = 2$ stack energies are in red/dashed line. The average separation between the levels is given on each plot. The plots that show the closest proximity sets are the B_2^-/A_2^+ and A_2^+/B_2^- sets, corresponding to the lower doublet of the 2's triplet. That large irregularity in the behavior of the $K_a = 2$ E_2^-/E_2^+ set is caused by an extremely large value for both the centrifugal distortion and asymmetry rotational constants and is further discussed later in the paper. The numerical values of the y-axis are arbitrarily removed for clarity of the figure.

resulting diagram for the upper state. Figure 6 is reproduced from Ref. 51 and shows the energy level diagram for vibrations with both A′ and A″ symmetry. It can be seen from the figure that we have observed a 1's triplet at lower energy than the 2's triplet in the $K_a = 1$ stack, which confirms the A″ symmetry. Similarly, for the $K_a = 0$ stack, we have observed the ordering of the 1's triplet to be B_1, E, A_1 for the J = 0 level, which is also consistent with A″ vibrational symmetry. An identical argument was used to justify the A″ symmetry for the $K_a = 2$ stack. Together with combination differences, an upper state symmetry of A″ is unambiguously assigned.

For the water dimer, A″ vibrational symmetry is consistent with the donor torsion, acceptor twist, and out-of-plane bend intermolecular vibrations. As the former two have been previously measured at frequencies <200 cm^{-1}, it seems clear that the out-of-plane bend is the vibration we are observing here. Additionally, Ceponkus *et al.* observed the out-of-plane bend in their matrix isolation experiment to lie near 522.4 cm^{-1} which agrees very well with our value for the origin of the $K_a = 1$ stack of 523.7 cm^{-1}.[46] It must be noted, however, that there is a possibility of observing "hot" bands in He expansions due to incomplete vibrational relaxation, which could explain the structure of the remaining unassigned lines. It is unlikely that these "hot" bands affected the present assignment however, as the transitions that were assigned generally correspond to those with highest intensity, and the transitions originating from "hot" bands are expected to be weak.

An estimation of the band origin of the $K_a = 0$ subband can be obtained by considering two facts. The first being that the acceptor switching splitting is generally similar for subbands belonging to the same vibration, and additionally that it tends to decrease as K_a increases. Also, the origin of the $K_a = 0$ subband must be lower than that of the $K_a = 1$ subband, which was experimentally determined herein to be 523.7 cm^{-1}. Based on this the only statement we can confidently make about the origin of the $K_a = 0$ subband is that it lies lower than 523.7 cm^{-1} which would indicate an acceptor switching splitting of at least 15.9 cm^{-1} which would fit the trend of dramatically increased tunneling splitting in the librational manifold observed in this experiment. An estimate of the origin in the 522-523 cm^{-1} region seems reasonable and allows some tentative comparisons to theory and matrix isolation experiments, which can be seen in Table IV. If the measurement is to be consistent with previous measurements, we would expect the origin of the $K_a = 0$ level to be lower than the matrix isolation result and higher that the B3LYP anharmonic calculation which is a range of 514.9–522.4 cm^{-1}, but without verification we cannot definitively assign a band origin.

ANALYSIS

Molecular constants from the fit

From the fitted constants given in Table III, several interesting phenomena are evident. The first is that within a triplet,

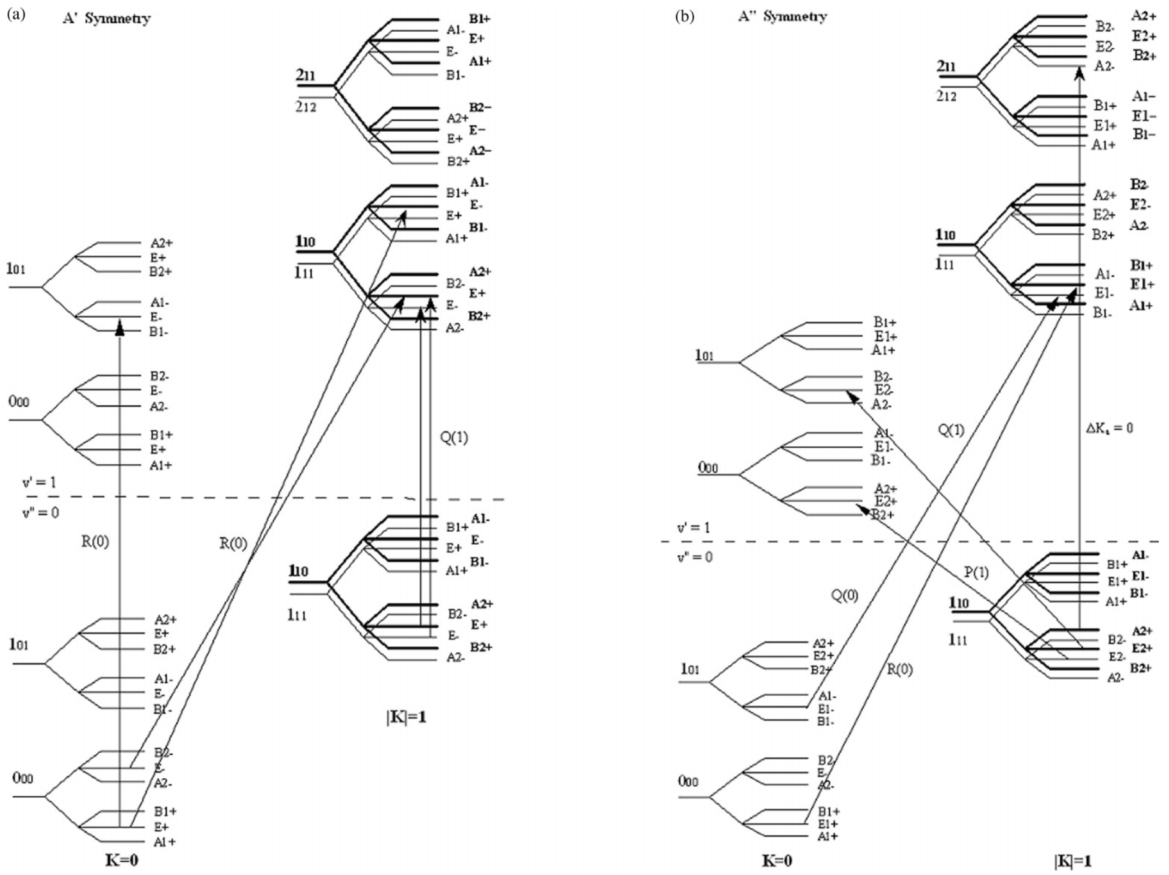

FIG. 6. Energy level diagram for excited state with A′ and A″ symmetry. Some possible transitions are shown for each upper state symmetry. Comparisons with Figure 3 provide evidence for the assignment to a vibration with A″ symmetry. Reproduced with permission from Harker *et al.*, Mol. Phys. **105**(5-7), 513–527 (2007). Copyright 2007 Taylor & Francis Group.

TABLE IV. Comparison of the fit constants of the excited state studied here with the water dimer ground state values.

	$K_a = 0$	
	Excited state	Ground state
B	6209–6236	6158–6166
D	0.144–0.911	0.036–0.050
	$K_a = 1$	
	Excited state	Ground state
B	6133–6270	6151–6167
D	−2.150 to −2.141	0.4895–0.542
Asymmetry	−88.450 to −11.126	1.255–15.732
d	−0.333 to −1.027	∼0.006
	$K_a = 2$	
	Excited state	Ground state
B	6105–6268	6142–6156
D	−1.566 to −5.763	0.039–0.051
Asymmetry	−5.660 to −0.499	∼0.001

the B rotational constants are generally quite consistent, whereas the other constants vary considerably, sometimes dramatically. For example, in the $K_a = 1$ stack, the B_2^-/A_2^+ set and A_2^+/B_2^- set have greatly increased values of D and d compared to the other sets in this triplet stack. A likely explanation is that these sets are nearly degenerate and may weakly perturb one other, leading to the irregular constants in Table II. As the constants of the other sets in the triplet have quite typical values for D and d, such a perturbation seems reasonable. Another interesting observation is the behavior of the E_2^-/E_2^+ set of the $K_a = 2$ stack. As seen in Figure 4, the predicted upper state energies for the upper state E_2^-/E_2^+ have a large degree of variability compared to the other plotted upper states. This is a manifestation of the abnormally large D and asymmetry constant for that set compared to the other sets in the stack. The exact cause of this is not obvious, but the most reasonable explanation is that there is some external perturbation affecting those energy levels, but the source of that perturbation is not yet clear.

Overall, the excited state constants from the fit are larger in magnitude than the corresponding constants in the ground state. Table IV presents a comparison of the upper state and ground state values, with the ground state constants taken from Ref. 30. The most striking difference between the two states is the dramatic increase in spread of measured constants in the upper state. Such variability in previous analyses has evidenced perturbations, e.g., Coriolis perturbation between the acceptor twist and acceptor wag vibrations as presented by Braly *et al.*[29] However, as mentioned earlier, the upper states in close proximity showed no evidence of Coriolis perturbations, which indicates that the perturbations must arise from some external levels. Based on calculations on the CC-pol-5s/f PES in the 475-600 cm^{-1} region, there is a large density of states at these energies, and even if the region is filtered by artificially "freezing" the states to 4 K, there still exist a large number of possible excited states predicted in the region, as shown in Figure 7. The large number of remaining unassigned transitions in the region constitutes further support for this notion. As the librational band is considered to be essential for understanding the hydrogen bond-breaking dynamics of liquid water, these perturbations clearly warrant further investigation as to their origin.

Additional insight into the behavior of the energy levels is obtained from the correlation matrices of the fits. For the $K_a = 0$ upper state, all B constants show a positive correlation with their respective D constants, whereas no correlation was observed between the constants and the tunneling magnitudes (as expected). The correlation for the $K_a = 1$ and $K_a = 2$ upper states the correlations are more interesting. Almost all of the states show the same correlation pattern, that is, the B constant is correlated positively to the D constant and the asymmetry constant is positively correlated to the d constant. In the case of the $K_a = 2$ levels, only the B and D constants are positively correlated. However, the lower triplet level for both $K_a = 1$ and $K_a = 2$ shows strong positive correlation between all constants involved in the fit. This could be evidence for some perturbation strongly affecting these levels. Considering that these levels are in near-degeneracy, as shown in Figure 4, this correlation can be again rationalized by an external perturbation. The only other remarkable observation in the correlation matrices is that for the $K_a = 2$, E_2^-/E_2^+ set there is a strong negative correlation between the D constants and the asymmetry constants, whereas the B constant is uncorrelated. This is not replicated by any other energy level set in the fit. As we stated above, the $K_a = 2$, E_2^-/E_2^+ set behaves very irregularly compared to the other sets and this correlation pattern serves as still further evidence that something is perturbing these levels.

As a final note, the traditional interpretation of the rotational constants in terms of nuclear coordinates and motions is inapplicable here, given the large magnitude of these constants compared to ground state values. However, this increased magnitude testifies that the water dimer is a highly nonrigid complex and that with excitations into the librational band of water the complex may display a particularly high degree of flexibility. An important conclusion to draw from

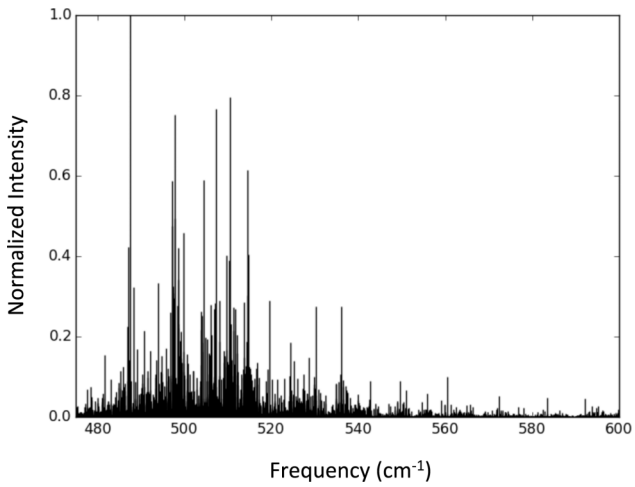

FIG. 7. Theoretical spectrum of $(H_2O)_2$ calculated on the CCpol-8s PES at a temperature of 4 K.

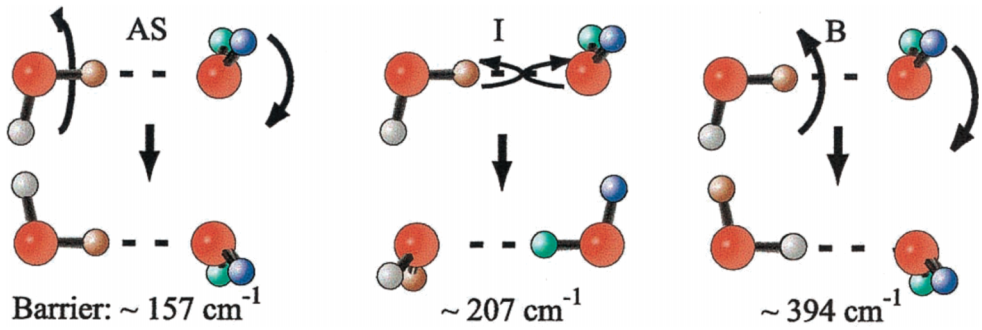

FIG. 8. The tunneling pathways of the water dimer along with the potential barriers calculated from the VRT(ASP-W) potential energy surface. The three tunneling pathways are shown: (AS) acceptor switching, (I) interchange tunneling, and (B) bifurcation tunneling. The associated motions of the pathways are also shown. By direct comparison to the motions of the intermolecular vibrations in Figure 1 of this paper, it can be see that some tunneling pathways are analogous to the motions of these vibrations: coupling of these vibrations to the tunneling motion would produce greatly increased experimental splittings/shifts. Reproduced with permission from F. N. Keutsch and R. J. Saykally, Proc. Natl. Acad. Sci. U. S. A. 98(19), 10 533–10 540 (2001). Copyright 2001 National Academy of Sciences.

this observation is that when simulating this region of the bulk (the librational band), flexible monomer models should be used.

Tunneling splittings

As all three tunneling pathways have now been characterized for the librational excitation, a comparison with the ground state values leads to a more complete understanding of the pathways and the associated tunneling barriers. In general, all of the measured values for the tunneling splittings in the librationally excited state show a dramatic increase over their ground state values. This is consistent with the results for previously studied lower energy excitations; however, the increases observed here—particularly for the bifurcation and interchange tunneling pathways—provide interesting new insights. Since only one acceptor switching splitting was measured, comparison to the ground state is tentative, pending further investigation; however, the observed value of ~308 GHz for the $K_a = 1$ stack greatly exceeds the value of ~83 GHz for the $K_a = 1$ stack of the ground state and is comparable to the value for the $K_a = 0$ ground state stack of 333 GHz. The enhanced acceptor switching is evidence for a reduced potential barrier in the excited state.

The observed interchange tunneling splittings range from 60 to 120 GHz, which again dramatically exceed the ground state values, all of which are less than 23 GHz. As for acceptor switching, the barrier for this pathway is very much less than 500 cm^{-1}; however, an additional factor may lead to the increased splittings. As shown in Figure 8, the tunneling motions closely resemble some of the intermolecular vibrations. Coupling of these vibrational motions to the tunneling pathways would lead to greatly increased splittings/shifts.[28,29]

The lowest barrier mechanism for interchange tunneling is the "geared" interchange pathway, consisting of a rotation of the donor molecule about the axis including the hydrogen bond, while the acceptor molecule rotates about its molecular C_2 axis. The donor then rotates about its molecular C_2 axis while the original acceptor rotates into the symmetry plane to become the new donor. The motion of the original donor molecule closely mirrors the motion of the out-of-plane libration, thus, coupling of the two motions is likely to produce an enhanced interchange tunneling. Such an enhancement could lead to increased splitting not consistent with simply transcending the tunneling barrier.

For bifurcation tunneling, the pathway is one that results in the exchange of the donor hydrogens. This motion appears to be strongly coupled to the out-of-plane libration. As the observed bifurcation shifts range from 2500 to 23 800 MHz (compared to ground state values estimated to be >750 MHz) this motion produces the most dramatic increase in tunneling effects relative to the ground state yet observed. In fact, the shifts are the highest ever measured for the bifurcation pathway for any water dimer, with the exception of the Coriolis-coupled acceptor wag and acceptor twist levels, where the abnormal shift was effected by the strong Coriolis interaction. Given that the excited state characterized here resides in the librational band region of liquid water, these increased tunneling splittings/shifts deserve further investigation as to their effects on hydrogen bond dynamics in liquid water.

One final intriguing consequence of the large interchange and bifurcation tunneling effects is the permutation of the usual ordering of the energy levels. Figure 9 shows a comparison of the expected and observed eigenstate ordering for two representative levels. The extent of the permutation varies but is more dramatic in the levels that have larger interchange and bifurcation tunneling perturbations, as would be expected. The effects of this permutation on the hydrogen bond dynamics of liquid and solid water could be interesting.

SUMMARY OF WATER VRT STUDIES

We have recently reviewed the experimental studies made for the water dimer.[20] Description of the currently observed VRT levels for $(H_2O)_2$ and $(D_2O)_2$ can be found in papers by Braly *et al.*, the early work in the microwave, the later work by Harker *et al.*, and complete characterization of the ground state by Keutsch *et al.*[28–32,51,52] These papers present observations of all the intermolecular vibrations except the in-plane and out-of-plane librations, the latter described herein.

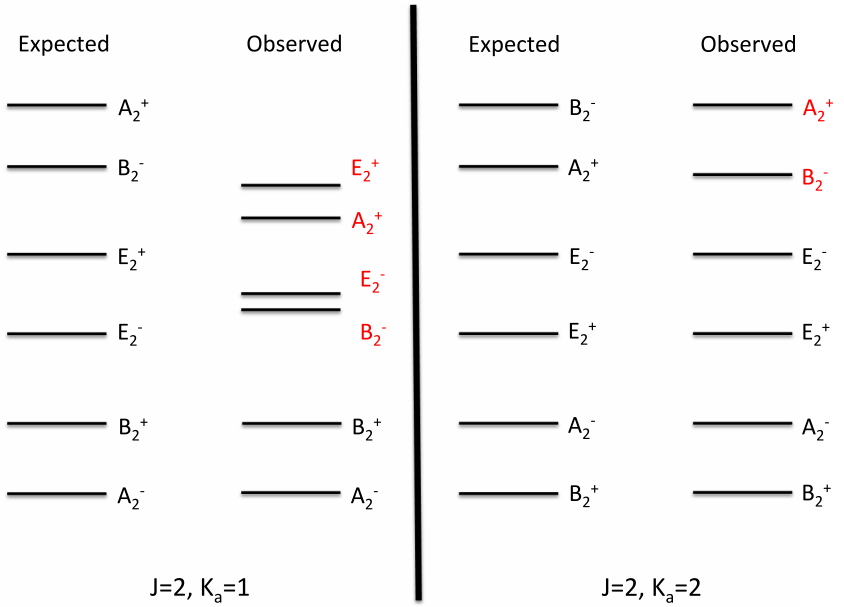

FIG. 9. Example of the permutation of energy level order. Drawing is done to relative scale. Levels permuted from their expected order are highlighted in red.

Tables V and VI show the results of the VRT experiments from the Saykally group together with matrix isolation measurements and various theoretical calculations of the intermolecular vibrations of both $(H_2O)_2$ and $(D_2O)_2$.

With this extensive collection of accurate spectroscopic data, sampling a large range of the dimer potential energy surface, it should now be possible to develop highly accurate potential models through direct inversion methods and thereby obtain the two-body interaction term in the many body expansion of bulk water potentials very accurately. Nevertheless, some experimental work remains to be done to completely characterize the fundamental intermolecular vibrations. The region of 300 cm^{-1} is particular interesting due to the observation of the in-plane libration in matrix isolation experiments.[46] The limited availability of suitable radiation sources in the terahertz region has traditionally been the limitation on VRT experiments with water clusters but emerging technologies may soon mitigate this problem.[53] In any case, the realization of a truly complete characterization of the water dimer is clearly near at hand.

TABLE V. Values for $(H_2O)_2$ intermolecular vibrations. Values shown for VRT experiments correspond to the band origin of the $K_a = 0$ subband, unless otherwise stated (due to incomplete spectral coverage, some values remain missing). Values for matrix isolation experiments and B3LYP anharmonic density functional theory (DFT) calculations are taken from Ref. 46. Values for CC-pol-8s/f and MB-pol are taken from Ref. 1 and correspond to the band origin of the $K_a = 0$ subband. All values are given in cm^{-1}.

Out-of-plane bend	VRT expt.	523.7 ($K_a = 1$)[a]	In-plane bend	VRT expt.	n/a
	Matrix isolation expt.	522.4		Matrix isolation expt.	309.1
	B3LYP anharmonic	514.9		B3LYP anharmonic	306.8
	SAPT-5st harmonic	564.7		SAPT-5st harmonic	367.0
	CC-pol-8s/f	n/a		CC-pol-8s/f	n/a
	MB-pol	n/a		MB-pol	n/a
O–O stretch	VRT expt.	153.62 ($K_a = 0$, 2's)	Acceptor twist	VRT expt.	120.19 ($K_a = 0$, 2's)
	Matrix isolation expt.	173.0		Matrix isolation expt.	150.6
	B3LYP anharmonic	124.4		B3LYP anharmonic	117.7
	SAPT-5st harmonic	186.8		SAPT-5st harmonic	143.7
	CC-pol-8s/f	146.4		CC-pol-8s/f	124.8
	MB-pol	151.9		MB-pol	124.3
Acceptor wag	VRT expt.	108.41	Donor torsion	VRT expt.	64.52 ($K_a = 0$, 2's)
	Matrix isolation expt.	122.2		Matrix isolation expt.	116
	B3LYP anharmonic	117.4		B3LYP anharmonic	77.5
	SAPT-5st harmonic	157.9		SAPT-5st harmonic	121.0
	CC-pol-8s/f	108.5		CC-pol-8s/f	87.3
	MB-pol	108.6		MB-pol	87.6

[a]Reported herein.

TABLE VI. Values for $(D_2O)_2$ intermolecular vibrations. Values shown for VRT experiments correspond to the band origin of the $K_a = 0$ subband, unless otherwise stated (Due to incomplete spectral coverage, some values remain missing). Values for matrix isolation experiments and B3LYP anharmonic DFT calculations are taken from Ref. 46. Values for CC-pol-8s/f are taken from Ref. 9 and correspond to the band origin of the $K_a = 0$ subband. All values are given in cm^{-1}. Values for the MB-pol potential are currently being investigated.

	VRT expt.	n/a		VRT expt.	n/a
	Matrix isolation expt.	393.2		Matrix isolation expt.	233.5
Out-of-plane bend	B3LYP anharmonic	396.0	In-plane bend	B3LYP anharmonic.	246.3
	SAPT-5st harmonic	406.1		SAPT-5st harmonic	274.8
	CC-pol-8s/f	n/a		CC-pol-8s/f	n/a
	VRT expt.	n/a		VRT expt.	91.64
	Matrix isolation expt.	166		Matrix isolation expt.	123.1
O–O stretch	B3LYP anharmonic	145.0	Acceptor twist	B3LYP anharmonic	105.1
	SAPT-5st harmonic	172.8		SAPT-5st harmonic	102.8
	CC-pol-8s/f	145.4		CC-pol-8s/f	89.9
	VRT expt.	83.52		VRT expt.	67.49
	Matrix isolation expt.	93.3		Matrix isolation expt.	87.7
Acceptor wag	B3LYP anharmonic	100.0	Donor torsion	B3LYP anharmonic	83.3
	SAPT-5st harmonic	118.5		SAPT-5st harmonic	88.1
	CC-pol-8s/f	81.7		CC-pol-8s/f	65.4

CONCLUSIONS

We have presented the first high resolution spectroscopy results characterizing the out-of-plane bend intermolecular vibration of $(H_2O)_2$ in the librational band region of liquid water. The excited states exhibit dramatic increases in tunneling splittings compared to the ground state, resulting in a permutation of the energy level ordering. A fit of the assigned transitions yields rotational constants that vary significantly from the ground state values, possibly the result of perturbations from the high density of energy levels that exist in the sampled frequency domain (ca. 500 cm^{-1}).

This work extends the characterization of the hydrogen bond vibrations of the water dimer to encompass five of the six intermolecular modes. Along with the recent measurement of the dimer dissociation energy,[54] this will enable rigorous tests of existing and future dimer potential surfaces, and hence, important progress in the determination of a new class of accurate models for solid and liquid water. Further work remains, however, to characterize the predicted 300 cm^{-1} in-plane librational motion.

ACKNOWLEDGMENTS

The Berkeley Terahertz spectroscopy effort is supported by the Chemical Structure, Dynamics, and Mechanisms A Division of the National Science Foundation under Grant No. 1300723. Part of this work was funded by the Agence Nationale de la Recherche Grant No. ANR-12-BS08-0010-01.

[1]V. Babin, C. Leforestier, and F. Paesani, "Development of a "First Principles" water potential with flexible monomers: Dimer potential energy surface, VRT spectrum, and second virial coefficient," J. Chem. Theory Comput. **9**(12), 5395–5403 (2013).

[2]R. S. Fellers, C. Leforestier, L. B. Braly, M. G. Brown, and R. J. Saykally, "Spectroscopic determination of the water pair potential," Science **284**, 945 (1999).

[3]M. P. Hodges, A. J. Stone, and S. S. Xantheas, "Contribution of many-body terms to the energy for small water clusters: A comparison of *ab initio* calculations and accurate model potentials," J. Phys. Chem. A **101**(48), 9163–9168 (1997).

[4]E. M. Mas, R. Bukowski, K. Szalewicz, G. C. Groenenboom, P. E. S. Wormer, and A. van der Avoird, "Water pair potential of near spectroscopic accuracy. I. Analysis of potential surface and virial coefficients," J. Chem. Phys. **113**(16), 6687 (2000).

[5]C. Millot and A. Stone, "Towards an accurate intermolecular potential for water," Mol. Phys. **77**(3), 439–462 (1992).

[6]N. Goldman, R. S. Fellers, M. G. Brown, L. B. Braly, C. J. Keoshian, C. Leforestier, and R. J. Saykally, "Spectroscopic determination of the water dimer intermolecular potential-energy surface," J. Phys. Chem. **116**(23), 10148 (2002).

[7]C. Leforestier, "Water dimer equilibrium constant calculation: A quantum formulation including metastable states," J. Chem. Phys. **140**(7), 074106 (2014).

[8]C. Leforestier, F. Gatti, R. S. Fellers, and R. J. Saykally, "Determination of a flexible (12D) water dimer potential via direct inversion of spectroscopic data," J. Phys. Chem. **117**(19), 8710 (2002).

[9]C. Leforestier, K. Szalewicz, and A. van der Avoird, "Spectra of water dimer from a new *ab initio* potential with flexible monomers," J. Chem. Phys. **137**(1), 014305 (2012).

[10]R. Bukowski, K. Szalewicz, G. C. Groenenboom, and A. van der Avoird, "Predictions of the properties of water from first principles," Science **315**(5816), 1249–1252 (2007).

[11]X. Huang, B. J. Braams, J. M. Bowman, R. E. Kelly, J. Tennyson, G. C. Groenenboom, and A. van der Avoird, "New *ab initio* potential energy surface and the vibration-rotation-tunneling levels of $(H_2O)_2$ and $(D_2O)_2$," J. Chem. Phys. **128**(3), 034312 (2008).

[12]R. E. A. Kelly, J. Tennyson, G. C. Groenenboom, and A. van der Avoird, "Water dimer vibration–rotation tunnelling levels from vibrationally averaged monomer wavefunctions," J. Quant. Spectrosc. Radiat. Transfer **111**(9), 1262–1276 (2010).

[13]J. C. Howard, J. L. Gray, A. J. Hardwick, L. T. Nguyen, and G. S. Tschumper, "Getting down to the fundamentals of hydrogen Bonding: Anharmonic vibrational frequencies of $(HF)_2$ and $(H_2O)_2$ from *ab initio* electronic structure computations," J. Chem. Theory Comput. **10**(12), 5426–5435 (2014).

[14]J. C. Howard and G. S. Tschumper, "Benchmark structures and harmonic vibrational frequencies near the CCSD(T) complete basis set limit for small water clusters: (H_2O) n = 2, 3, 4, 5, 6," J. Chem. Theory Comput. **11**(5), 2126–2136 (2015).

[15]G. S. Tschumper, M. L. Leininger, B. C. Hoffman, E. F. Valeev, H. F. Schaefer, and M. Quack, "Anchoring the water dimer potential energy surface with explicitly correlated computations and focal point analyses," J. Chem. Phys. **116**(2), 690 (2002).

[16]A. Shank, Y. Wang, A. Kaledin, B. J. Braams, and J. M. Bowman, "Accurate *ab initio* and "hybrid" potential energy surfaces, intramolecular vibrational

energies, and classical ir spectrum of the water dimer," J. Chem. Phys. **130**(14), 144314 (2009).
[17]T. R. Dyke, "Group theoretical classification of the tunneling–rotational energy levels of water dimer," J. Chem. Phys. **66**(2), 492 (1977).
[18]N. Goldman, C. Leforestier, and R. J. Saykally, "A 'first principles' potential energy surface for liquid water from VRT spectroscopy of water clusters," Philos. Trans. R. Soc., A **363**(1827), 493–508 (2005).
[19]C. Leforestier, L. B. Braly, K. Liu, M. J. Elrod, and R. J. Saykally, "Fully coupled six-dimensional calculations of the water dimer vibration-rotation-tunneling states with a split Wigner pseudo spectral approach," J. Chem. Phys. **106**(20), 8527 (1997).
[20]A. Mukhopadhyay, W. T. S. Cole, and R. J. Saykally, "The water dimer I: Experimental characterization," Chem. Phys. Lett. **633**, 13–26 (2015).
[21]N. Pugliano and R. J. Saykally, "Measurement of the ν8 intermolecular vibration of $(D_2O)_2$ by tunable far infrared laser spectroscopy," J. Chem. Phys. **96**(3), 1832 (1992).
[22]F. N. Keutsch and R. J. Saykally, "Water clusters: Untangling the mysteries of the liquid, one molecule at a time," Proc. Natl. Acad. Sci. U. S. A. **98**(19), 10533–10540 (2001).
[23]M. J. Smit, G. C. Groenenboom, P. E. S. Wormer, and A. van der Avoird, "Vibrations, tunneling, and transition dipole Moments in the water dimer," J. Phys. Chem. A **105**, 6212 (2001).
[24]A. D. Buckingham, J. E. Del Bene, and S. A. C. McDowell, "The hydrogen bond," Chem. Phys. Lett. **463**(1-3), 1–10 (2008).
[25]L. H. Coudert and J. T. Hougen, "Tunneling splittings in the water dimer: Further development of the theory," J. Mol. Spectrosc. **130**, 86 (1988).
[26]L. H. Coudert and J. T. Hougen, "Analysis of the microwave and far infrared spectrum of the water dimer," J. Mol. Spectrosc. **139**, 259 (1990).
[27]H. C. Longuet-Higgins, "The symmetry groups of non-rigid molecules," Mol. Phys. **6**(5), 445–460 (1963).
[28]L. B. Braly, J. D. Cruzan, K. Liu, R. S. Fellers, and R. J. Saykally, "Terahertz laser spectroscopy of the water dimer intermolecular vibrations I. $(D_2O)_2$," J. Chem. Phys. **112**(23), 10293 (2000).
[29]L. B. Braly, K. Liu, M. G. Brown, F. N. Keutsch, R. S. Fellers, and R. J. Saykally, "Terahertz laser spectroscopy of the water dimer intermolecular vibrations II. $(H_2O)_2$," J. Chem. Phys. **112**(23), 10314 (2000).
[30]F. N. Keutsch, N. I. R. Goldman, H. A. Harker, C. Leforestier, and R. J. Saykally, "Complete characterization of the water dimer vibrational ground state and testing the VRT(ASP-W)III, SAPT-5st, and VRT(MCY-5f) surfaces," Mol. Phys. **101**(23-24), 3477–3492 (2003).
[31]L. H. Coudert, F. J. Lovas, R. D. Suenram, and J. T. Hougen, "New measurements of microwave transitions in the water dimer," J. Chem. Phys. **87**(11), 6290 (1987).
[32]R. D. Suenram, G. T. Fraser, and F. J. Lovas, "Microwave spectrum of $(D_2O)_2$," J. Mol. Spectrosc. **138**, 440 (1989).
[33]F. N. Keutsch, R. S. Fellers, M. G. Brown, M. R. Viant, P. B. Petersen, and R. J. Saykally, "Hydrogen bond breaking dynamics of the water trimer in the translational and librational band region of liquid water," J. Am. Chem. Soc. **123**, 5938 (2001).
[34]H. Bakker J., S. Woutersen, and H.-K. Nienhuys, "Reorientational motion and hydrogen-bond stretching dynamics in liquid water," Chem. Phys. **258**, 233 (2000).
[35]A. Luzar and D. Chandler, "Structure and hydrogen bond dynamics of water-dimethyl sulfoxide mixtrues by computer siulatons," J. Chem. Phys. **98**(10), 8160 (1993).
[36]A. Luzar and D. Chandler, "Effect of environment on hydrogen bond dynamics in liquid water," Phys. Rev. Lett. **76**(6), 928 (1996).
[37]F. N. Keutsch, J. D. Cruzan, and R. J. Saykally, "The water trimer," Chem. Rev. **103**, 2533 (2003).
[38]L. M. Goss, S. W. Sharpe, T. A. Blake, V. Vaida, and J. W. Brault, "Direct absorption spectroscopy of water clusters," J. Phys. Chem. A **103**, 8620 (1999).
[39]G. A. Blake, K. B. Laughlin, R. C. Cohen, K. L. Busarow, D.-H. Gwo, C. A. Schmuttenmaer, D. W. Steyert, and R. J. Saykally, "The Berkeley tunable far infrared laser spectrometers," Rev. Sci. Instrum. **62**(7), 1701 (1991).
[40]G. A. Blake, K. B. Laughlin, R. C. Cohen, K. L. Busarow, D.-H. Gwo, C. A. Schmuttenmaer, D. W. Steyert, and R. J. Saykally, "Tunable far infrared laser spectrometers," Rev. Sci. Instrum. **62**(7), 1693 (1991).
[41]K. Liu, R. S. Fellers, M. R. Viant, R. P. McLaughlin, M. G. Brown, and R. J. Saykally, "A long path length pulsed slit valve appropriate for high temperature operation: Infrared spectroscopy of jet-cooled large water clusters and nucleotide bases," Rev. Sci. Instrum. **67**(2), 410 (1996).
[42]F. N. Keutsch, R. S. Fellers, M. R. Viant, and R. J. Saykally, "Far-infrared laser vibration–rotation–tunneling spectroscopy of water clusters in the librational band region of liquid water," J. Phys. Chem. **114**(9), 4005 (2001).
[43]K. von Puttkamer and M. Quack, "High resolution interferometric FTIR spectroscopy of $(HF)_2$: Analysis of a low frequency fundamental near 400 cm^{-1}," Mol. Phys. **62**(5), 1047–1064 (1987).
[44]J. Ceponkus, A. Engdahl, P. Uvdal, and B. Nelander, "Structure and dynamics of small water clusters, trapped in inert matrices," Chem. Phys. Lett. **581**, 1–9 (2013).
[45]J. Ceponkus and B. Nelander, "Water dimer in solid Neon. Far-infrared spectrum," J. Phys. Chem. A **108**(31), 6499–6502 (2004).
[46]J. Ceponkus, P. Uvdal, and B. Nelander, "Intermolecular vibrations of different isotopologs of the water dimer: Experiments and density functional theory calculations," J. Chem. Phys. **129**(19), 194306 (2008).
[47]J. Ceponkus, P. Uvdal, and B. Nelander, "Far-infrared band strengths in the water dimer: Experiments and calculations," J. Phys. Chem. A **112**(17), 3921–3926 (2008).
[48]H. A. Harker, F. N. Keutsch, C. Leforestier, Y. Scribano, J. X. Han, and R. J. Saykally, "Toward a precise determination of the acceptor switching splitting in the water dimer," Mol. Phys. **105**(5-7), 497–512 (2007).
[49]See supplementary material at http://dx.doi.org/10.1063/1.4933116 for correlation matrices of fits.
[50]T. A. Hu and T. R. Dyke, "Water dimer Coriolis resonances and Stark effects," J. Chem. Phys. **91**(12), 7348 (1989).
[51]H. A. Harker, F. N. Keutsch, C. Leforestier, Y. Scribano, J. X. Han, and R. J. Saykally, "Refinements in the description of excited VRT states of the water dimer," Mol. Phys. **105**(5-7), 513–527 (2007).
[52]F. N. Keutsch, L. B. Braly, M. G. Brown, H. A. Harker, P. B. Petersen, C. Leforestier, and R. J. Saykally, "Water dimer hydrogen bond stretch, donor torsion overtone, and in-plane bend vibrations," J. Chem. Phys. **119**(17), 8927 (2003).
[53]W. T. S. Cole, N. C. Hlavacek, A. W. M. Lee, T.-Y. Kao, Q. Hu, J. L. Reno, and R. J. Saykally, "A Terahertz VRT spectrometer employing quantum cascade lasers," Chem. Phys. Lett. **638**, 144–148 (2015).
[54]L. C. Ch'ng, A. K. Samanta, G. Czako, J. M. Bowman, and H. Reisler, "Experimental and theoretical investigations of energy transfer and hydrogen-bond breaking in the water dimer," J. Am. Chem. Soc. **134**(37), 15430–15435 (2012).